Structural and Metabolic Specificity of Methylthiocoformycin for Malarial Adenosine Deaminases

ARTICLE *in* BIOCHEMISTRY · OCTOBER 2009

Impact Factor: 3.02 · DOI: 10.1021/bi9012484

8 AUTHORS, INCLUDING:

Meng-Chiao Ho
Academia Sinica
24 PUBLICATIONS **354** CITATIONS
SEE PROFILE

Maria Belen Cassera
Virginia Polytechnic Institute and State Univ…
40 PUBLICATIONS **491** CITATIONS
SEE PROFILE

Peter C Tyler
Victoria University of Wellington
196 PUBLICATIONS **4,082** CITATIONS
SEE PROFILE

Kami Kim
Albert Einstein College of Medicine
111 PUBLICATIONS **3,188** CITATIONS
SEE PROFILE

Published in final edited form as:
Biochemistry. 2009 October 13; 48(40): 9618–9626. doi:10.1021/bi9012484.

Structural and metabolic specificity of methylthiocoformycin for malarial adenosine deaminases†

Meng-Chiao Ho[‡,¶], **María B. Cassera**[‡,¶], **Dennis C. Madrid**[§], **Li-Min Ting**[§,∥], **Peter C. Tyler**[⊥], **Kami Kim**[§,∥], **Steven C. Almo**[‡], and **Vern L. Schramm**[‡,*]

[‡]Department of Biochemistry, Yeshiva University, Bronx, New York 10461, USA. [§]Department of Microbiology and Immunology, Yeshiva University, Bronx, New York 10461, USA. [∥]Medicine Albert Einstein College of Medicine, Yeshiva University, Bronx, New York 10461, USA. [⊥]Carbohydrate Chemistry Group, Industrial Research Ltd., Lower Hutt, New Zealand

Abstract

Plasmodium falciparum is a purine auxotroph requiring hypoxanthine as a key metabolic precursor. Erythrocyte adenine nucleotides are the source of the purine precursors, making adenosine deaminase (ADA) a key enzyme in the pathway of hypoxanthine formation. Methylthioadenosine (MTA) is a substrate for most malarial ADAs, but not for human ADA. The catalytic site specificity of malarial ADAs permits methylthiocoformycin (MT-coformycin) to act as a *Plasmodium*-specific transition state analogue with low affinity for human ADA (Tyler, P. C., Taylor, E. A., Fröhlich, R. G. G. and Schramm, V. L. (2007) *J. Am. Chem. Soc. 129*, 6872–6879). The structural basis for MTA and MT-coformycin specificity in malarial ADAs is the subject of speculation (Larson, E. T. et al. (2008) *J. Mol. Biol. 381*, 975–988). Here, the crystal structure of ADA from *Plasmodium vivax* in complex with MT-coformycin reveals an unprecedented binding geometry for 5’-methylthioribosyl groups in the malarial ADAs. Compared to malarial ADA complexes with adenosine or deoxycoformycin, 5’-methylthioribosyl groups are rotated 130°. A hydrogen bonding network between Asp172 and the 3'-hydroxyl of MT-coformycin is essential for recognition of the 5’-methylthioribosyl group. Water occupies the 5'-hydroxyl binding site when MT-coformycin is bound. Mutagenesis of Asp172 destroys the substrate specificity for MTA and MT-coformycin. Kinetic, mutagenic and structural analyses of *Pv*ADA and kinetic analysis of five other plasmodial ADAs establishes the unique structural basis for its specificity for MTA and MT-coformycin. *Plasmodium gallinaceum* ADA does not use MTA as a substrate, is not inhibited by MT-coformycin and is missing Asp172. Treatment

†This work was supported by NIH Research Grants AI049512, Training Grants F31 AI05665 and CM007288, U.S. Army Research Grant W81XWH-05-2-0025 and in part by a contract from the Medicines in Malaria (MMV) Consortium, Geneva, Switzerland. Parts of this manuscript were published in a thesis submitted by DCM in partial fulfillment of the requirements for the Degree Doctor of Philosophy in the Sue Golding Graduate Division of Medical Sciences, Albert Einstein College of Medicine, Yeshiva University. Data of X-ray diffraction for this study were measured at Beamline X29A of the National Synchrotron Light Source and Beamline 24-ID-E at the Northeastern Collaborative Access Team Beamlines of the Advanced Photon Source. Financial support of Beamline X29A of the National Synchrotron Light Source comes principally from the Offices of Biological and Environmental Research and of Basic Energy Sciences of the US Department of Energy, and from the National Center for Research Resources the National Institutes of Health. The Northeastern Collaborative Access Team Beamlines of the Advanced Photon Source is supported by award RR-15301 from the National Center for Research Resources at the National Institute of Health. Use of the Advanced Photon Source is supported by the U.S. Department of Energy, Office of Basic Energy Sciences, under Contract No. DE-AC02-06CH11357.

*To whom correspondence should be addressed: Department of Biochemistry, Jack and Pearl Resnick Campus, 1300 Morris Park Ave., Bronx, NY 10461. Telephone: (718) 430-2813. Fax: (718) 430-8565. vern@aecom.yu.edu.
¶Contributed equally to this study.

SUPPORTING INFORMATION AVAILABLE

Primer sequences used for cloning of adenosine deaminase from different *Plasmodium* species and primer sequences used for site-directed mutagenesis of *P. vivax* ADA. Sequence alignment of plasmodial and mammalian ADAs. This material is available free of charge via the Internet at http://pubs.acs.org.

of *P. falciparum* cultures with coformycin or MT-coformycin in the presence of MTA is effective in inhibiting parasite growth.

Malaria is caused by protozoan parasites of the *Plasmodium* genus. Within the four species of malaria parasite that infect humans, *Plasmodium vivax* and *Plasmodium falciparum* are the most prevalent species, with *P. falciparum* being responsible for most of the fatal cases (1). *P. vivax* has the widest global distribution and is responsible for most of the malaria cases in Central and South America and Asia (2). *Plasmodium knowlesi* is a primate malaria that is an emerging infectious disease of humans (3,4). Malaria treatment by chemotherapeutic and vector control strategies have not prevented its widespread occurrence. Recent increases in the resistance of malaria parasites to drug treatment and in mosquito vectors to insecticides have renewed the demand for new chemotherapeutic strategies (5,6). The 48 hr intraerythrocytic parasite growth phase requires robust nucleic acid synthesis, thus, targeting of purine salvage pathways provide a promising route for novel drug development.

All *Plasmodium* species are purine auxotrophs, salvaging host cell purines for synthesis of cofactors and nucleic acids (7,8). In *Plasmodium*, adenosine is converted to hypoxanthine using adenosine deaminase (ADA) and purine nucleoside phosphorylase (PNP). IMP is formed from hypoxanthine by hypoxanthine-guanine-xanthine phosphoribosyl-transferase (HGXPRT). Inhibition of the purine salvage pathway with transition state analogue inhibitors of both human and *Plasmodium* PNP, such as Immucillin-H and 4’-deaza-1’-aza-2’-deoxy-1’-(9-methylene)-Immucillin-G (DADMe-ImmG), are lethal for *P. falciparum in vitro* (9,10).

Coformycin is a picomolar, transition state analogue inhibitor of both human and *Plasmodium* ADAs (11). Coformycin alone does not inhibit parasite growth in cultured erythrocytes (10) but 2’-deoxycoformycin (d-coformycin, Pentostatin) is reported to cause decreased parasitemia in *P. knowlesi*-infected primates (12). *Plasmodium* species lack adenosine kinase (10,13) and cannot incorporate exogenous adenosine directly into the adenylate pool. Thus, adenosine (or MTA) can only be salvaged after action of ADA in the parasite. Here, we demonstrate that *P. falciparum in vitro* growth is inhibited by coformycin or MT-coformycin with MTA as the purine source.

P. falciparum ADA (*Pf*ADA) also deaminates 5’-methylthioadenosine (MTA; Figure 1) in addition to adenosine (14). Thus, *P. falciparum* ADA serves the dual functions of adenosine salvage and recycling MTA formed from the synthesis of polyamines (14). Mammalian ADAs do not deaminate MTA and instead express a specific MTA phosphorylase for recycling of MTA (14). Mammalian erythrocytes do not synthesize polyamines. Thus, an intact polyamine synthetic pathway is important for the viability of malaria parasites (14,15). In *P. falciparum*, MTA is deaminated by *Pf*ADA to 5’-methylthioinosine (MTI), a metabolite that has not been reported in mammalian metabolism (16). The *Plasmodium* PNP also serves a dual purpose by converting both inosine and MTI to hypoxanthine for conversion to IMP and incorporation into nucleic acids (14).

We synthesized 5’-methylthiolcoformycin (MT-coformycin; Figure 1) as a specific transition state analogue inhibitor of plasmodial ADAs based on their unusual specificity for both adenosine and MTA (11). MT-Coformycin is a sub-nanomolar inhibitor of *Pf*ADA and demonstrates >20,000 fold selectivity for *Pf*ADA relative to human ADA. This selectivity is remarkable since coformycin and d-coformycin are powerful picomolar inhibitors of both human and *P. falciparum* ADAs (11).

To understand the structural basis of recognition of *Pf*ADA for MTA and MT-coformycin, we overexpressed and characterized five additional ADAs from parasites with different host preferences: *P. vivax* (human), *P. knowlesi* (*P. falciparum*-like; simian host), *P. cynomolgi*

(*P. vivax*-like; simian host), *P. berghei* (rodent host) and *P. gallinaceum* (avian host). Avian erythrocytes are nucleated, distinguishing them from mammalian red cells. Within the six plasmodial ADAs tested, only *P. gallinaceum* ADA (*Pg*ADA) does not have significant activity for MTA and consequently, MT-coformycin is a poor inhibitor. Sequence alignment revealed that *Pg*ADA differs in its catalytic site with an Asp172Glu replacement.

Recent crystal structures of *P. vivax* ADA (*Pv*ADA) revealed catalytic site interactions with adenosine and d-coformycin (17). Molecular modeling experiments hypothesized that the *Plasmodium* species enzymes can accommodate the 5'-methylthio substituent with only minor conformational changes to the catalytic site amino acids and to the ligand (17).

Here, we present the crystal structure of MT-coformycin bound to *Pv*ADA at 2.1 Å resolution. MT-Coformycin binds tightly as a consequence of a large change in the glycosidic torsion angle to reposition the 5'-methylthioribosyl group in a geometry previously unseen in other adenosine deaminases structures (17,18). The 1.9 Å resolution crystal structure and kinetic properties of a mutant lacking Asp172 (*Pv*ADA-ΔAsp172) established the mechanism of MT-coformycin binding.

EXPERIMENTAL PROCEDURES

Cloning and expression of adenosine deaminase enzymes from different Plasmodium species

Orthologs of *Pf*ADA were located using the tblastn function (default settings) with the *P. knowelsi*, *P. vivax*, *P. reichenowi*, *P. gallinaceum*, and *P. berghei* genome sequence databases from Sequencing Groups at the Sanger Institute (http://www.sanger.ac.uk/pathogens/malaria/), The Institute for Genomic Research Parasite Database (http://www.tigr.org/parasiteProjects.shtml) and PlasmoDB (http://plasmodb.org/). Appropriate primers were designed (Supporting information, Table S1). *P. cynomolgi* ADA was cloned using degenerate primers based on the *P. reichenowi* sequence. In each strain ADA was predicted to reside on a contiguous DNA sequence to permit cloning from genomic DNA. Genomic DNA from *P. berghei* (ANKA strain), *P. vivax* (Sal-1, gift of Jane Carlton, NYU Langone Medical Center), *P. gallinaceum* (gift of Joseph Vinetz, UCSD School of Medicine), *P. cynomolgi* and *P. knowlesi* (gift of Clemens Kocken and Alan Thomas, Biomedical Primate Research Centre) was used for PCR amplification of the ADA gene from each species. The coding region of each enzyme, without the stop codon, was amplified by PCR and cloned into the pTrcHis2-TOPO vector (Invitrogen) with a C-terminal His_6 tag and ampicillin selection cassette. Each plasmid was transformed into *E. coli* strain TOP10 (Invitrogen) and multiple clones of each DNA encoding for ADA were sequenced and the data confirmed from the *P. knowlesi*, *P. vivax*, *P. gallinaceum* and *P. berghei* genome predictions. The DNA sequence for *P. cynomolgi* ADA was determined and is reported as new data since no genome sequence data was available. The respective amino acid sequences of the malarial ADAs are reported (Supporting information, Figure S1). The recombinant enzymes were expressed by induction of 100 ml bacterial culture with 1 mM isopropyl-1-thio-β-D-galactopyranoside (IPTG) at 37 °C for 18 h and purified using nickel-nitrilotriacetic acid affinity chromatography (Ni-NTA spin column, Qiagen) according to the manufacturer's instructions. The purified proteins were used for enzymatic assays without further purification. Enzyme concentrations were determined from the extinction coefficients at 280 nm (Supporting information, Table S1).

P. falciparum in vitro cell growth and inhibition assay

Coformycin and MT-coformycin were dissolved in water. Inhibition tests were carried out in flat-bottomed microtiter plates (Costar). The method described by Desjardins and colleagues (19) was used to determine the IC_{50} value and parasite DNA content was determined by DNA

dye-binding fluorescence as described by Quashie and colleagues (20). For each condition, three experiments were carried out in duplicate. Synchronized *P. falciparum* cultures were grown in purine-rich medium (370 μM hypoxanthine, standard medium). Prior to growth inhibition experiments, schizont stage parasite cultures were split and one half was washed in purine-free medium and cultured in purine-free medium for 24 h while the other half was maintained in standard medium. Ring stage parasite cultures (200 μl per well, with 1% hematocrit and 1% parasitemia) were grown for 72 h in the presence of increasing inhibitor concentration in the presence of 100 μM MTA as sole purine source. After incubation, cells were harvested and analyzed for DNA content. Uninfected erythrocytes were used as background controls.

Site-directed mutagenesis of P. vivax ADA

Site-directed mutagenesis used the QuickChange® Site-directed Mutagenesis kit (Stratagene) according to the manufacturer's instructions. Appropriate primers were designed (Supporting information, Table S2) and the mutagenesis reactions were performed using the pTcrHis2-TOPO vector containing the *Pv*ADA sequence as the template. The final reaction mixture was transformed into *E. coli* strain X10-Gold (Stratagene). Multiple clones of each ADA mutant were sequenced to confirm the presence of the desired mutation (Supporting information, Table S2). The plasmids carrying the desired mutations were transformed into *E. coli* strain BL21-codon plus (DE3)-RIPL (Stratagene). The recombinant enzymes were expressed, purified and quantified as described above.

Enzymatic assays and inhibition studies

Recombinant proteins were used for enzymatic assays directly following purification. Adenosine deaminase activity was determined by monitoring the change in absorbance at 265 nm upon conversion of adenosine to inosine or MTA to MTI in 100 mM Tris-HCl buffer (pH 8.0) and varied concentrations of adenosine or MTA (14). Enzyme inhibition assays to determine the K_i value for initial and slow-onset inhibition constants (K_i^*) were performed using different concentration of coformycin or MT-coformycin (generous gifts of Peter C. Tyler, Industrial Research, Ltd., New Zealand) and 200 μM adenosine. The inhibition constants were determined as described previously (11).

Protein purification and crystallization

Recombinant *Pv*ADA and the mutant *Pv*ADA-ΔAsp172 were expressed by induction of the bacterial culture with 1 mM IPTG at 30 °C for 18 h. The cells were ruptured by passage through a French press, the cell debris was removed by centrifugation, and the remaining supernatant was purified over a 3 ml Ni-NTA affinity column with elution by a step gradient of 10, 50, 75, 100 and 500 mM imidazole. Purified recombinant proteins were dialyzed overnight against 50 mM HEPES pH 7.5, 50 mM NaCl and 1 mM DTT. The final concentration of wild type *Pv*ADA for crystallization was 10 mg/ml in the presence of 1 mM MT-coformycin. The crystallization condition of 25% PEG3350, 100 mM Hepes pH 7.5 and 0.2 M $MgCl_2$ was identified using Hampton Research Index HT screening by sitting-drop vapor diffusion. A condensed cluster of rod-shaped crystals was obtained. *Pv*ADA-ΔAsp172 (10 mg/ml) failed to co-crystallize with MT-coformycin but co-crystallized with 3 mM MTA in 0.2 M $MgCl_2$, 0.1 M BisTris pH 5.5 and 25% PEG 3350. MTA was not present in the co-crystallized crystal (data not shown). These crystals were soaked with 2 mM MT-coformycin for 1 hour to obtain MT-coformycin bound to *Pv*ADA-ΔAsp172. Crystals were transferred into a fresh drop of the crystallization solution containing 20% glycerol and rapidly frozen in liquid nitrogen.

Data collection and processing

X-ray diffraction data of MT-coformycin bound to *Pv*ADA was collected at Beamline 24-ID-E equipped with a MD-2 microdiffractometer at the Advanced Photo Source of Argonne National Laboratory. The microdiffractometer was used to search for a well separated diffraction pattern among the crystal cluster. X-ray diffraction of MT-coformycin bound *Pv*ADA-ΔAsp172 was collected at Beamline X29A at Brookhaven National Laboratory. All data were processed with HKL2000 program suite and the data processing statistics are provided in Table 1 (21).

Structure determination and refinement

The crystal structure of *Pv*ADA bound to MT-coformycin was determined by molecular replacement in Molrep (22) using the published structure of *Pv*ADA bound to d-coformycin (PDB:2PGR) as the search model. The model without MT-coformycin and Zn^{2+} ion was first built in COOT (23) and refined in Refmac5. The Zn^{2+} ion was added and refined based on the crystal studies by Larson and colleagues (17). The MT-coformycin was added last using the Fo-Fc map and refined in Refmac5 (24). The crystal structure of *Pv*ADA-ΔAsp172 bound to MT-coformycin was determined in the same way as the crystal structure of *Pv*ADA bound to MT-coformycin. In both crystal structures, His 253 and Asp310 coordinate the catalytic zinc ion and are the only residues whose torsion angles are in the disallowed region of the Ramachandron plot. The disfavored torsion angles of His254 and Asp310 are also observed and described in the other three published structures of *Pv*ADA with bound ligands (17). The final models were validated by Procheck in the absence of the disordered residues, including the first six amino acid residues and C-terminal linker with the his-tag (25) and the refinement statistics were summarized in Table 1. The ligand-omit mF_o-DF_c difference map and ligand-omit $2mF_o$-DF_c electron density map, presented in figure 4C and 5C were calculated using phases from the final refined protein models from which the ligands were removed (26). Figure 3A, 4, 5, 6 and 7, where oxygen, nitrogen and sulfur atoms were colored in red, blue and magenta, respectively were made by Pymol (http://www.pymol.org).

RESULTS

Identification and characterization of ADA from various Plasmodium species

Open reading frames for ADA from various *Plasmodium* species were identified, placed in expression vectors and the expressed proteins were purified to characterize the kinetic parameters, substrate and inhibitor specificity. *P. falciparum* was used as a control since it had been previously characterized (11,14). The *Plasmodium* ADA amino acid sequences (Supporting information, Figure S1) exhibit identity values ranging from 62% to 72% as compared to *Pf*ADA. The K_m values for adenosine ranged from 32 μM (*P. gallinaceum*) to 120 μM (*P. knowlesi*) while the K_m values for MTA varied from 4.4 μM (*P. berghei*) to 115 μM (*P. falciparum*) and had no detectable catalytic activity with *P. gallinaceum* ADA (Table 2). All ADAs had k_{cat}/K_m values near 10^4 $M^{-1}s^{-1}$ with adenosine as substrate. Similar values were obtained with MTA as a substrate with the exception of *Pg*ADA which showed no detectable activity for MTA under conditions that would have detected 0.1% of that activity.

The K_i values for coformycin ranged from 2.3 nM (*P. berghei*) to 14 nM (*P. falciparum*) and the K_i^* (slow-onset inhibition constant) varied from 0.25 nM (*P. berghei*) to 0.71 nM (*P. vivax*). Inhibition constants for MT-coformycin ranged from 3.2 nM (*P. falciparum*) to 48 nM (*P. knowlesi*) and showed no detectable inhibition with *P. gallinaceum*. Only *Pf*ADA and *Pb*ADA showed slow-onset inhibition for MT-coformycin, to give K_i^* values of 0.25 and 5 nM, respectively (Table 3).

Effect of coformycin and MT-coformycin on P. falciparum DNA biosynthesis

The effect of inhibiting parasite ADA or parasite plus host ADAs was measured in *P. falciparum* 3D7 strain cultured in human erythrocytes. DNA content was analyzed following treatment with coformycin (inhibitor of both human and parasite ADAs) or MT-coformycin (inhibitor of parasite ADA) for 72 hr in the presence of MTA. The inhibitors reduced parasite DNA synthesis with IC_{50} values of 2 nM for coformycin and 5 nM for MT-coformycin when 100 μM MTA was provided as the exogenous purine source (Figure 2). Adenosine and MTI were also tested as exogenous purine source but no inhibition was detected (data not shown).

Characterization of PvADA mutants

Based on the crystal structure of *Pv*ADA with bound MT-coformycin (see below) three *Pv*ADA mutants were designed (Supporting information, Table S2) to test the importance of Asp172 in methylthio-group recognition. Kinetic constants were determined under the same conditions as the *Pv*ADA wild-type (Table 4). All Asp172 mutants lost the ability to deaminate MTA and lost their high affinity for MT-coformycin. *Pv*ADA-Glu172 showed weak catalytic activity at elevated enzyme concentration (data not shown). In contrast to the loss of 5'-methylthio group specificity, deletion of Asp172 produced only a small effect on the catalytic efficiency for adenosine and the binding of coformycin.

Structure of PvADA with MT-coformycin

The structure of *Pv*ADA in complex with MT-coformycin was solved and refined to final resolution of 2.1 Å. *Pv*ADA is a typical TIM barrel, composed of eight α-helices and eight β-strands plus 16 α-helices of accessory structure. With MT-coformycin bound in the active site, the Asp172-Ile180 region (part of the β3 strand and β3/α12 loop) shifts approximately 15 Å compared to the open structure reported for apo *P. yoelli* ADA (17). This movement forms a closed foot-shaped cavity in the active site with the 2'- and 3'-hydroxyl groups of the MT-coformycin in the heel portion of the foot shaped cavity (Figure 3A).

Geometry of MT-Coformycin in PvADA

The 8-*R*-hydroxy-diazepine ring of MT-coformycin mimics the 6-*R*-hydroxyl tetrahedral Meisenheimer intermediate, similar to the transition state formed by water attack at C6 of adenosine. The 8-*R*-hydroxy-group of MT-coformycin replaces the attacking water nucleophile and is chemically stable since the position normally occupied by the leaving group amine in the adenosine transition-state is replaced by a hydrogen. This hydrogen is facing the solvent, consistent with solvent water acting as the proton donor to NH_2 to form the NH_3 leaving group. The diazepine ring is positioned near the toe of a foot-shaped cavity (Figure 3), where in addition to the zinc ion interactions, N1H of the ring donates a hydrogen bond to Glu229. This is a specific transition state interaction since in the normal reaction, N1 of adenosine is a H-bond acceptor while at the transition state, it is rehybridized to N1H to become a H-bond donor, as in the bound MT-coformycin. His253, Asp310 and Asp311 and the backbone of Gly201 interact with MT-coformycin similar to the interactions with adenosine, the normal substrate (Figure 4A and 4C).

The 5'-methylthio group is displaced from the 5'-hydroxyl group binding site and is replaced by a structurally defined water molecule held in place by hydrogen bonds with His44, Asp46 and the 2'- and 3'-hydroxyl groups of MT-coformycin (Figure 3A and Figure 4A). The 3'-hydroxyl group of MT-coformycin also hydrogen bonds with Asp172. This geometry of hydrogen bonds requires a 130° rotation of the ribosyl group around the glycosyl torsion angle (Table 5) with respect to bound adenosine (17). The position of the 5'-methylthio group (Figures 4A and 4B) causes it to be positioned almost 180° relative to the 5'-hydroxyl group found with bound adenosine, guanosine and d-coformycin (17). Despite the dramatic alteration

of the MT-ribose group geometry with respect to bound ribosyl groups, only a slight shift of the diazepine ring (approximately 0.4 Å) occurs relative to the position of d-coformycin in the active site (Figure 4A and 4B). These changes place the 5'-methylthio group near the ankle region of the foot-shaped cavity, directed toward to protein surface (Figure 3A). The 5'-methylthio group fits closely into a hydrophobic cavity without room for crystallographically ordered water molecules. The geometry of bound MT-coformycin provides a sharp contrast to adenosine, guanosine and d-coformycin where the 5'-hydroxyl group hydrogen bonds with His44 and Asp46 and points toward the protein core (Figures 4A and 4B).

MT-coformycin in the active site of PvADA-ΔAsp172

Based on the structural comparison between bovine ADA with bound 6-hydroxy-1,6-dihydropurine riboside, (Figure 5A, structure in gray) and *Pv*ADA with MT-coformycin bound, (Figure 5B, structure in yellow) and the primary sequence alignment between mammalian and plasmodial ADAs (Supplementary Figure S1), we hypothesized that an extra amino acid insertion into the *Pv*ADA is responsible for the observed conformational differences between mammalian and plasmodial ADAs. We deleted Asp172 of *Pv*ADA to shift Thr173 to the Thr172 position (Figures 5B and 5C). In mammalian ADAs, a Met is present at the equivalent position. The crystal structure of *Pv*ADA-ΔAsp172 in complex with MT-coformycin shows an open Asp172-Ile180 region (Figure 5A, structure in green), similar to bovine ADA in complex with the inhibitor (Figure 5A, structure in gray). In *Pv*ADA-ΔAsp172, with Thr172 now replacing the Asp group, the hydrogen bond with the 3'-hydroxyl group of MT-coformycin is lost (Figure 5B and 5C). In *Pv*ADA-ΔAsp172, the ribosyl group of MT-coformycin rotates to the orientation found for d-coformycin in *Pv*ADA (Figure 6). Phe132, located near His44 and Asp46, swings 30° away from the active site to accommodate the 5'-methylthio group (Figure 6). The unfavorable nature of this geometry for 5'-methylthioribose group binding is apparent in a 200-fold decrease in affinity for MT-coformycin (Table 4). The relative energetic contributions from methylthio and ribosyl group interactions are not available from these structures, but cause an approximate 3 kcal/mol energy loss.

DISCUSSION

Function of plasmodial and mammalian ADAs

Malarial parasites express relatively large quantities of ADA protein, suggesting its metabolic importance in the essential purine salvage pathway. Coformycin (10) and d-coformycin (27) are weak inhibitors of parasite growth in cultured erythrocytes but d-coformycin has been reported to decrease the parasitemia in primates infected with *P. knowlesi* (12). The action of ADA inhibitors *in vivo* suggests ADA as a potential target for antimalarials. ADA from *P. falciparum* also functions to deaminate MTA, a by-product of polyamine synthesis. In *Plasmodium*, ADA converts MTA to MTI and purine nucleoside phosphorylases converts MTI to hypoxanthine and 5-methylthio-α-D-ribose-1-phosphate. These enzymes form the only known pathway for MTA catabolism in *Plasmodium*, a necessary step for MTA recycling to methionine and *S*-adenosylmethionine. Human ADA has not evolved for MTA deamination activity since a methylthioadenosine phosphorylase (MTAP) and adenine phosphoribosyltransferase recycle the purine base in humans (28). Neither of these enzymes is encoded in *P. falciparum* genome (13). We tested the effect of coformycin and MT-coformycin in *P. falciparum* cultures in the presence of 100 μM MTA as an exogenous purine source (Figure 2). Under these conditions, coformycin and MT-coformycin reduce DNA synthesis of *P. falciparum in vitro* by approximately 80%, supporting plasmodial ADA as the pathway for MTA metabolism. Equivalent inhibition of DNA synthesis by coformycin and MT-coformycin establishes the parasite ADA as the target since coformycin is a pM inhibitor of host and parasite ADAs while MT-coformycin inhibits only the plasmodial ADA. Use of

MT-coformycin as a potential antimalarial avoids the neurotoxicity of ADA inhibitors (such as Pentostatin, d-coformycin) in humans (29).

Species specificity for MT-coformycin action

Other *Plasmodium* species were examined for the substrate specificity of their ADAs. *Plasmodium* parasites that infect mammals (*P. vivax, P. berghei, P. knowlesi* and *P. cynomolgi*) showed robust catalytic efficiency for both adenosine and MTA. In contrast, *P. gallinaceum* that infects bird erythrocytes had no significant catalytic ability with MTA and was not inhibited by MT-coformycin (Table 2 and Table 3). Avian erythrocytes differ from those in mammals in that they have an average life of 35 days, are nucleated, larger in size and oblate ellipsoid in shape. The presence of nucleus, ribosomes, Golgi and mitochondria creates a different metabolic environment for the malaria parasite, as purines and polyamines can be salvaged or synthesized *de novo* in avian erythrocytes (30). The ADA specificity of *P. gallinaceum* suggests that activity for MTA deamination is unnecessary in this parasite as no MTA would be formed within the parasites if polyamines are salvaged from the host. This species difference provides a convenient tool to explore the catalytic site elements involved in 5'-methylthio group recognition. As shown below, the replacement of Asp172 with Glu172 in *P. gallinaceum* is important in its restricted activity for 5'-methylthioribosyl groups.

ADA catalytic site determinants for MTA recognition

Based on the crystal structures, sequence alignment and mutagenesis (see below), Asp172 is essential for the methylthio-specificity (Table 4). The crystal structure of MT-coformycin bound to *Pv*ADA established a remarkable spatial re-arrangement of methylthio-derivates. Although most plasmodial ADAs bind both coformycin and MT-coformycin with pM affinity, the orientation of the 5'-methylthioribosyl group of MT-coformycin is altered relative to d-coformycin. In nucleosides and d-coformycin, the 5'-hydroxyl group is H-bonded to His44 and Asp46. The 5'-methylthio group is not accommodated in the 5'-hydroxyl binding site, and the ribose is rotated by 130° to permit the 3'-hydroxyl group to hydrogen bond to Asp172. The 5'-hydroxyl group is replaced by a water molecule and the 5'-methylthio group relocates to a more hydrophobic region of the catalytic site, near Phe132 (Fig. 6). This rotation and the Asp172 interaction with the 3'-hydroxyl group is critical to permit MT-coformycin and MTA binding. In plasmodial ADAs, an Asp172 signature at the 5'-binding site indicates the ability of ADAs to accept MTA as a substrate and to be inhibited by tight binding of MT-coformycin. In mammalian ADAs, Met152 occupies the residue equivalent to *Pv*ADA-ΔAsp172. Met152 prevents binding of 5'-methylthio-derivatives due to a spatial clash, and this region of the sequence is completely conserved in mouse, bovine and human ADAs (Figure 7).

Substrate and inhibitor interactions in plasmodial ADAs

Of the six species of plasmodial ADAs examined here, only *P. gallinaceum*, in which Asp172 is replaced by Glu, is catalytically inactive with MTA. Mutated *Pv*ADAs (Asp172Ala, Asp172Glu and ΔAsp172) show catalytic characteristics similar to *P. gallinaceum* ADA. The hydrogen bond between the 3'-hydroxyl group of methylthio-derivates and Asp172 is required to permit methylthio-derivative binding and thereby assist in anchoring the purine or diazepine rings. Critically, this geometric change in the methylthioribose occurs while still permitting the purine group to achieve alignment with the catalytic site Zn^{2+} as needed for activation of the water nucleophile at the reaction center. Without the hydrogen bond between the 3'-hydroxyl group and Asp172, the methylthioribosyl group adopts the ribosyl conformation found in adenosine and d-coformycin binding. In that case, the methylthio-group is unfavorably positioned in the hydrophilic pocket near Asp46, His44 and a crystallographic water site. Kinetic evidence for this ribosyl conformational shift comes from the 200-fold weaker inhibition of MT-coformycin for *Pv*ADA-ΔAsp172 than for *Pv*ADA. Likewise, the *P.*

gallinaceum ADA, containing Asp172Glu, binds MT-coformycin 14,500-fold weaker than *Pv*ADA.

Conclusion

Plasmodial ADAs are capable of using adenosine and MT-adenosine do so by accommodating the 5’-ribosyl and 5’-methylthioribosyl groups in different geometries. The 5’-ribosyl groups of substrates and inhibitors form hydrogen bonds with His44 and Asn46 in a 5’-hydroxyl group site. The 5’-methylthioribosyl substrates and inhibitors bind with the ribosyl groups in a different geometry with a hydrogen bond between the 3’-hydroxyl and Asp172. Mutation of Asp172 eliminates efficient deamination of MTA and MT-coformycin binding. A critical feature of this unusual geometrically-linked specificity in ADA is the ability to rotate the ribose groups of methylthioribosyl-derivatives in the active site of plasmodial ADAs while maintaining the register of the catalytic site elements with the site of hydrolytic deamination. Humans use MTAP to convert MTA to adenine and 5-methylthioribose 1-phosphate by phosphorolysis and human ADA does not deaminate MTA. *Plasmodium* has no MTAP and most species deal with MTA by deamination using the double-specificity ADAs featuring Asp172 as an essential catalytic site specificity element. A replacement of Asp172 on ADAs by intentional mutation causes loss of MTA deaminase activity and MT-coformycin binding. The absence of Asp172 in the case of *P. gallinaceum* has the same effect. Catalytic site flexibility in the malarial ADAs permits efficient purine metabolism with fewer expressed proteins.

Supplementary Material

Refer to Web version on PubMed Central for supplementary material.

Abbreviations

ADA, adenosine deaminase
MTA, methylthioadenosine
MT-coformycin, methylthiocoformycin
PNP, purine nucleoside phosphorylase
HGXPRT, hypoxanthine-guanine-xanthine phosphorobosyl transferase
IMP, inosine 5’-monophosphate
MTI, methylthioinosine
d-coformycin, 2’-deoxycoformycin
Asp, aspartic acid
Glu, glutamic acid
His, Histidine
Ala, alanine
Gly, glycine
Thr, threonine
Phe, phenylalanine
Met, methionine
Ile, isoleucine

REFERENCES

1. Snow RW, Guerra CA, Noor AM, Myint HY, Hay SI. The global distribution of clinical episodes of *Plasmodium falciparum* malaria. Nature 2005;434:214–217. [PubMed: 15759000]
2. Mendis K, Sina BJ, Marchesini P, Carter R. The neglected burden of *Plasmodium vivax* malaria. Am. J. Trop. Med. Hyg 2001;64:97–106. [PubMed: 11425182]

3. Jongwutiwes S, Putaporntip C, Iwasaki T, Sata T, Kanbara H. Naturally acquired *Plasmodium knowlesi* malaria in human, Thailand. Emerg. Infect. Dis 2004;10:2211–2213. [PubMed: 15663864]
4. Cox-Singh J, Davis TM, Lee KS, Shamsul SS, Matusop A, Ratnam S, Rahman HA, Conway DJ, Singh B. *Plasmodium knowlesi* malaria in humans is widely distributed and potentially life threatening. Clin. Infect. Dis 2008;46:165–171. [PubMed: 18171245]
5. Hyde JE. Drug-resistant malaria. Trends Parasitol 2005;21:494–498. [PubMed: 16140578]
6. Hyde JE. Drug-resistant malaria - an insight. Febs J 2007;274:4688–4698. [PubMed: 17824955]
7. de Koning HP, Bridges DJ, Burchmore RJ. Purine and pyrimidine transport in pathogenic protozoa: from biology to therapy. FEMS Microbiol. Rev 2005;29:987–1020. [PubMed: 16040150]
8. Hyde JE. Targeting purine and pyrimidine metabolism in human apicomplexan parasites. Curr. Drug Targets 2007;8:31–47. [PubMed: 17266529]
9. Kicska GA, Tyler PC, Evans GB, Furneaux RH, Schramm VL, Kim K. Purine-less death in *Plasmodium falciparum* induced by immucillin-H, a transition state analogue of purine nucleoside phosphorylase. J. Biol. Chem 2002;277:3226–3231. [PubMed: 11706018]
10. Cassera MB, Hazleton KZ, Riegelhaupt PM, Merino EF, Luo M, Akabas MH, Schramm VL. Erythrocytic adenosine monophosphate as an alternative purine source in *Plasmodium falciparum*. J. Biol. Chem 2008;283:32889–32899. [PubMed: 18799466]
11. Tyler PC, Taylor EA, Frohlich RF, Schramm VL. Synthesis of 5'-methylthio coformycins: specific inhibitors for malarial adenosine deaminase. J. Am. Chem. Soc 2007;129:6872–6879. [PubMed: 17488013]
12. Webster HK, Wiesmann WP, Pavia CS. Adenosine deaminase in malaria infection: effect of 2'-deoxycoformycin *in vivo*. Adv. Exp. Med. Biol 1984;165(Pt A):225–229. [PubMed: 6609525]
13. Gardner MJ, Hall N, Fung E, White O, Berriman M, Hyman RW, Carlton JM, Pain A, Nelson KE, Bowman S, Paulsen IT, James K, Eisen JA, Rutherford K, Salzberg SL, Craig A, Kyes S, Chan MS, Nene V, Shallom SJ, Suh B, Peterson J, Angiuoli S, Pertea M, Allen J, Selengut J, Haft D, Mather MW, Vaidya AB, Martin DM, Fairlamb AH, Fraunholz MJ, Roos DS, Ralph SA, McFadden GI, Cummings LM, Subramanian GM, Mungall C, Venter JC, Carucci DJ, Hoffman SL, Newbold C, Davis RW, Fraser CM, Barrell B. Genome sequence of the human malaria parasite *Plasmodium falciparum*. Nature 2002;419:498–511. [PubMed: 12368864]
14. Ting LM, Shi W, Lewandowicz A, Singh V, Mwakingwe A, Birck MR, Ringia EA, Bench G, Madrid DC, Tyler PC, Evans GB, Furneaux RH, Schramm VL, Kim K. Targeting a novel *Plasmodium falciparum* purine recycling pathway with specific immucillins. J. Biol. Chem 2005;280:9547–9554. [PubMed: 15576366]
15. Trackman PC, Abeles RH. Methionine synthesis from 5'-SMethylthioadenosine. Resolution of enzyme activities and identification of 1-phospho-5-S methylthioribulose. J. Biol. Chem 1983;258:6717–6720. [PubMed: 6853500]
16. Olszewski KL, Morrisey JM, Wilinski D, Burns JM, Vaidya AB, Rabinowitz JD, Llinas M. Host-parasite interactions revealed by *Plasmodium falciparum* metabolomics. Cell Host Microbe 2009;5:191–199. [PubMed: 19218089]
17. Larson ET, Deng W, Krumm BE, Napuli A, Mueller N, Van Voorhis WC, Buckner FS, Fan E, Lauricella A, DeTitta G, Luft J, Zucker F, Hol WG, Verlinde CL, Merritt EA. Structures of substrate- and inhibitor-bound adenosine deaminase from a human malaria parasite show a dramatic conformational change and shed light on drug selectivity. J. Mol. Biol 2008;381:975–988. [PubMed: 18602399]
18. Wang Z, Quiocho FA. Complexes of adenosine deaminase with two potent inhibitors: X-ray structures in four independent molecules at pH of maximum activity. Biochemistry 1998;37:8314–8324. [PubMed: 9622483]
19. Desjardins RE, Canfield CJ, Haynes JD, Chulay JD. Quantitative assessment of antimalarial activity in vitro by a semiautomated microdilution technique, *Antimicrob*. Agents Chemother 1979;16:710–718.
20. Quashie NB, de Koning HP, Ranford-Cartwright LC. An improved and highly sensitive microfluorimetric method for assessing susceptibility of *Plasmodium falciparum* to antimalarial drugs *in vitro*. Malar. J 2006;5:95. [PubMed: 17076900]

21. Otwinowski Z, Minor W. Processing of X-ray Diffraction Data Collected in Oscillation Mode. Methods in Enzymology 1997;276:307–326.
22. Vagin AA, Teplyakov A. MOLREP: an Automated Program for Molecular Replacement. J. Appl. Cryst 1997;30:1022–1025.
23. Emsley P, Cowtan K. Coot: model-building tools for molecular graphics. Acta Crystallogr. D Biol. Crystallogr 2004;60:2126–2132. [PubMed: 15572765]
24. Murshudov GN, Vagin AA, Dodson EJ. Refinement of macromolecular structures by the maximum-likelihood method, *Acta Crystallogr*. D Biol. Crystallogr 1997;53:240–255.
25. Laskowski RA, McArthur MW, Moss DS, Thornton JM. PROCHECK: a program to check the stereochemical quality of protein structures. J. Appl. Cryst 1993;265:283–291.
26. Read RJ. Improved Fourier coefficients for maps using phases from partial structures with errors. Acta Crystal 1986;A42:140–149.
27. Roth E Jr, Ogasawara N, Schulman S. The deamination of adenosine and adenosine monophosphate in *Plasmodium falciparum*-infected human erythrocytes: *in vitro* use of 2'deoxycoformycin and AMP deaminase-deficient red cells. Blood 1989;74:1121–1125. [PubMed: 2665862]
28. Singh V, Schramm VL. Transition-state structure of human 5'-methylthioadenosine phosphorylase. J. Am. Chem. Soc 2006;128:14691–14696. [PubMed: 17090056]
29. Sauter C, Lamanna N, Weiss MA. Pentostatin in chronic lymphocytic leukemia. Expert Opin. Drug Metab. Toxicol 2008;4:1217–1222. [PubMed: 18721115]
30. Stevens, L. Avian Biochemistry and molecular biology. New York: Cambridge University Press; 1996.

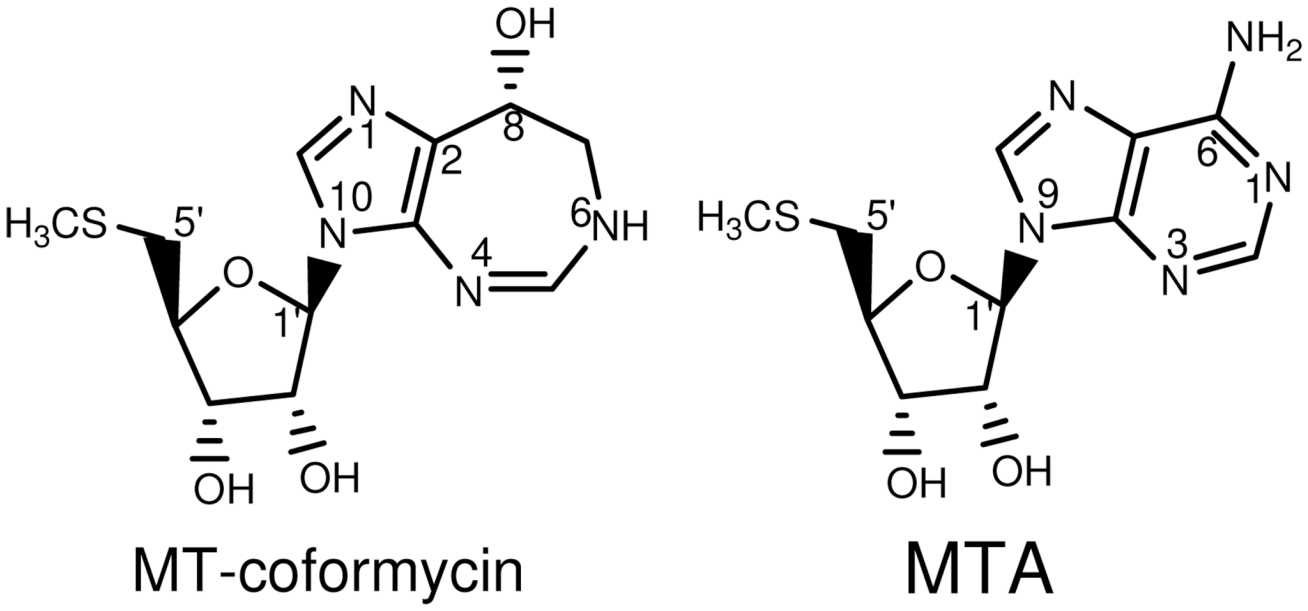

Figure 1.
Structures and atomic numbering for MT-coformycin and methylthioadenosine (MTA).

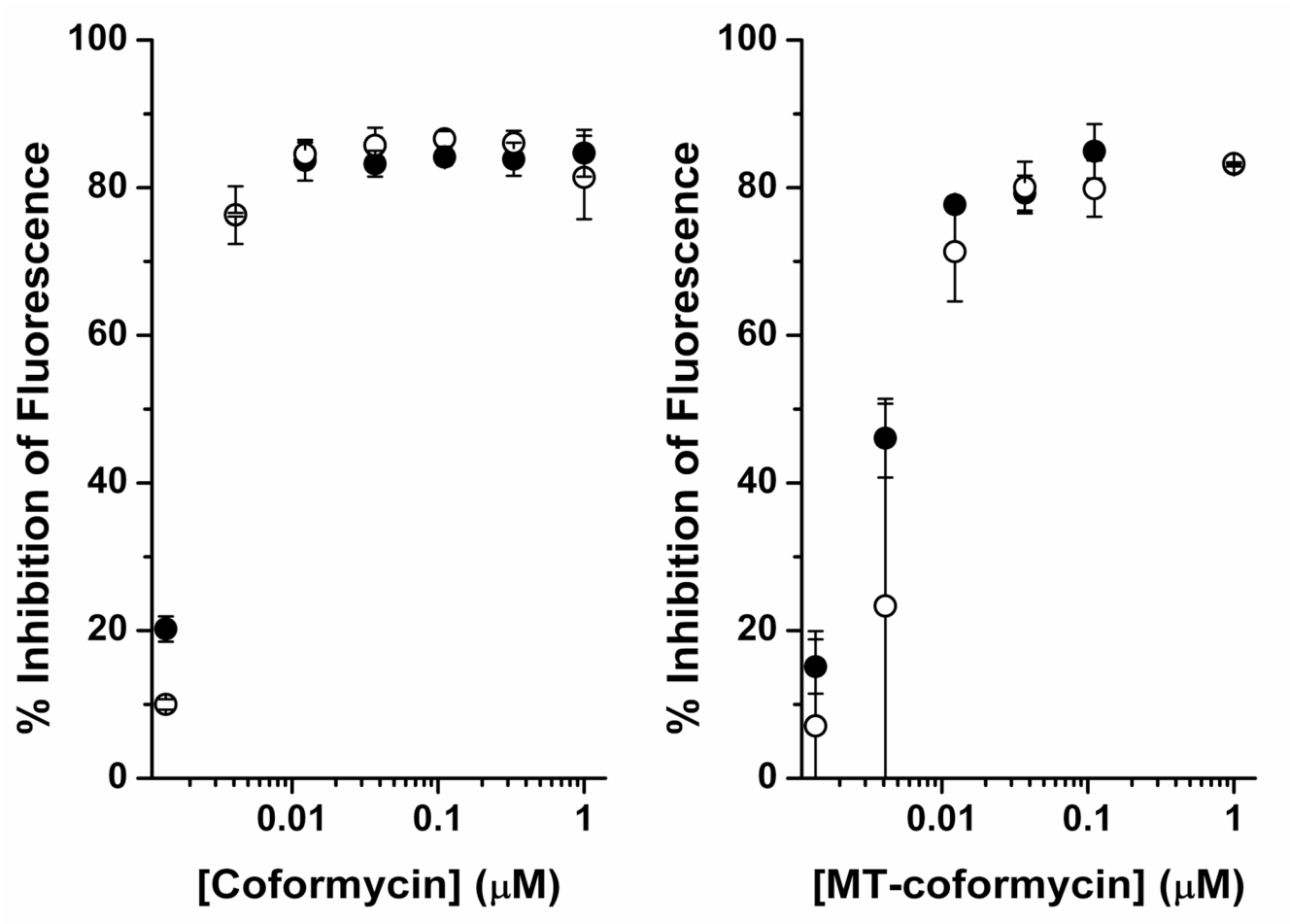

Figure 2.

Inhibition of DNA synthesis in *P. falciparum* cultures treated with coformycin and MT-coformycin. Infected erythrocytes were cultured in the presence of 100 μM MTA in the presence of the indicated inhibitor concentrations for 72 hr, followed by DNA analysis. Means and standard deviations are from 3 independent experiments. Open circles: culture was incubated in purine-free medium prior to addition of the inhibitor. Closed circles: cultures were maintained in purine-rich medium until treatment. All treatments were performed in media containing MTA as the sole exogenous purine source.

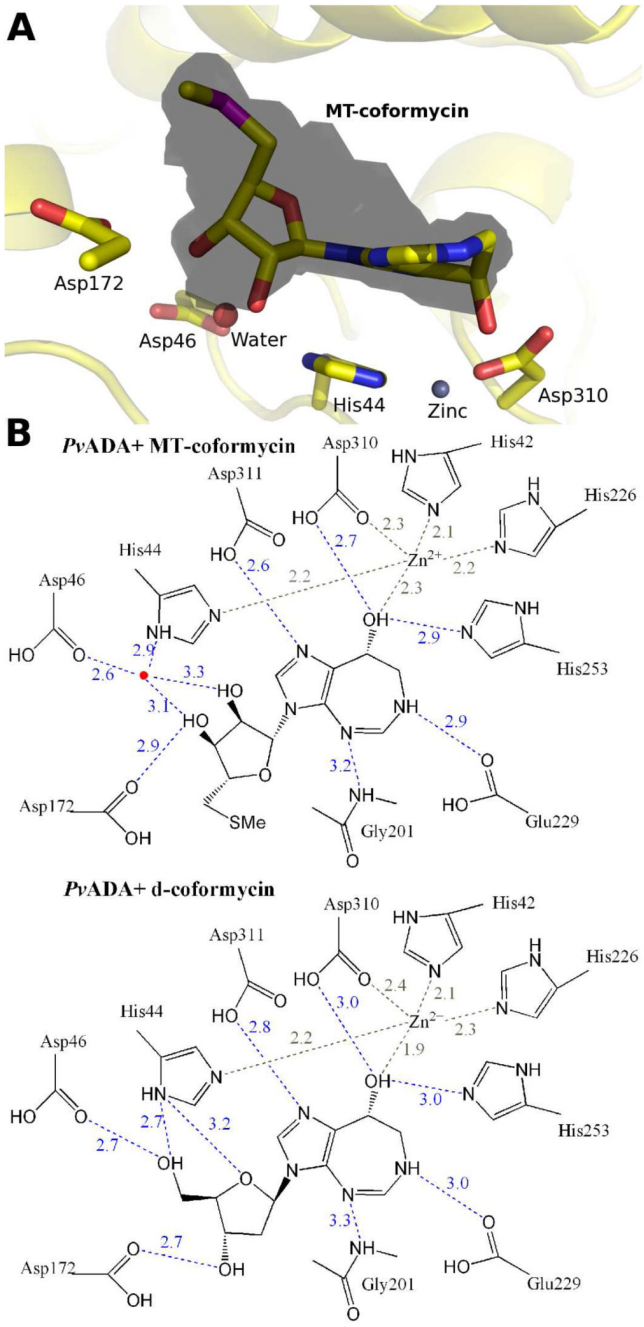

Figure 3.

A: The solvent accessible surface map of a cut-surface diagram of *Pv*ADA with bound MT-coformycin. The solvent accessible map (colored in gray) shows an enclosed cavity comprising the active site of *Pv*ADA. The 5'-methylthiol group of MT-coformycin (shown in the surface map) fits tightly into this cavity. The side chains of Asp172, His42, Asp45 and a structural water are shown. The water molecule replaces the 5'-hydroxyl group of adenosine when 5'-methylthioribosyl groups are bound. The side chain of Asp172 is in hydrogen-bond contact to the 3'-hydroxyl group. **B:** The relative position of MT-coformycin (this study) is compared to d-coformycin (PDB ID: 2PGR) and the active site residues of *Pv*ADA. The water molecule is

drawn as a red dot. The hydrogen bonds and zinc ion interactions are depicted in blue and gray dashed lines (Å), respectively.

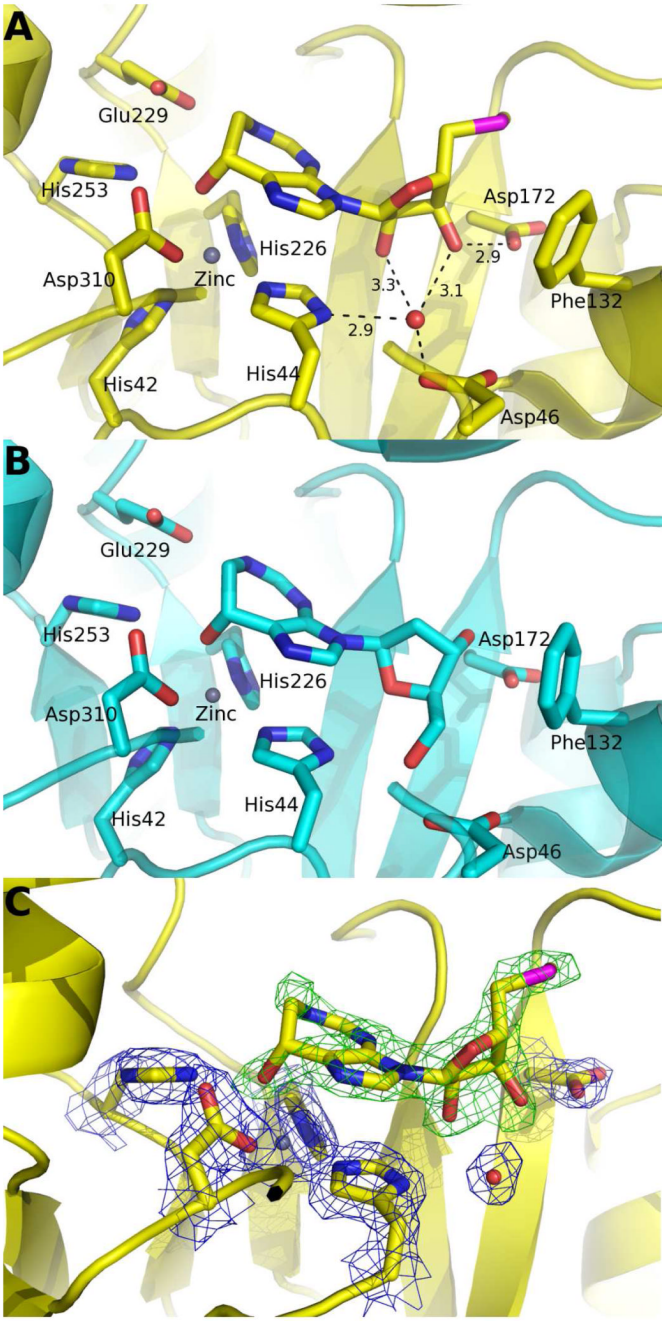

Figure 4.

The comparative geometry of MT-coformycin and d-coformycin in the active site of *Pv*ADA. **A**: MT-coformycin in the catalytic site of *Pv*ADA is colored in yellow. The hydrogen bonds between the ribosyl group of MT-coformycin and adjacent catalytic site molecules are shown as dashed lines and distances are given in Å. The Zn^{2+} ion is shown in gray. **B**: The position of d-coformycin bound to *Pv*ADA is shown in blue and the Zn^{2+} ion in gray. **C**: The ligand-omit electron density map of MT-coformycin bound *Pv*ADA. The MT-coformycin-omit mF_o-DF_c difference map was shown in green at a contour level of 3.0 σ and MT-coformycin-omit $2mF_o$-DF_c electron density map of His44, His226, His253, Asp172, Asp310 and a structural water was drawn in blue at a contour level of 1.4σ.

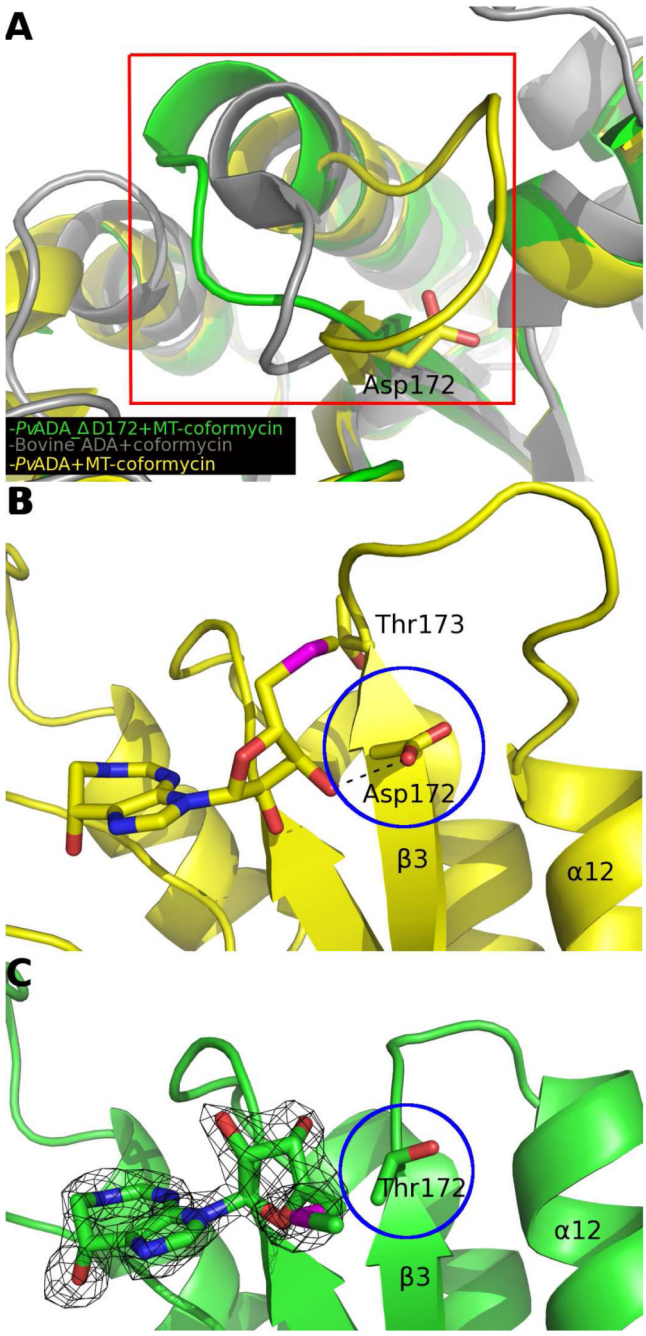

Figure 5.

The Asp172-Ile180 region of ADA structures consisting of *Pv*ADA with MT-coformycin, bovine ADA with 6-hydroxy-1,6-dihydropurine riboside and *Pv*ADA-ΔAsp172 with MT-coformycin. **A:** Inhibitor-bound ADAs are depicted as ribbon diagrams and colored in yellow (*Pv*ADA), gray (bovine ADA; PDB ID: 1KRM) and green (PvADA-ΔAsp172). To indicate the position of the active site, Asp172 of MT-coformycin bound *Pv*ADA is shown. The *Plasmodium*-specific Asp172-Ile180 from *Pv*ADA is enclosed in the red box. The *Plasmodium*-specific region of inhibitor-bound *Pv*ADA-ΔAsp172 bears greater structural resemblance to the equivalent region of inhibitor-bound bovine ADA than to *Pv*ADA. **B:** An expanded view of the *Plasmodium*-specific region of MT-coformycin-bound *Pv*ADA. **C:** An

expanded view of the *Plasmodium*-specific region of MT-coformycin-bound *Pv*ADA-ΔAsp172. The MT-coformycin-omit mF_o-DF_c difference map was drawn in black at a contour level of 3.0 σ. MT-coformycin and the side chains of Asp172, Thr173 and Ile180 are depicted as stick models. The hydrogen bonding interaction between Asp172 and *Pv*ADA-bound MT-coformycin is represented by a dashed line. The deletion of Asp172 results in a reorganization of the *Plasmodium*-specific region in *Pv*ADA-ΔAsp172 that includes shortening of the β3 strand and elongation of the α12 helix.

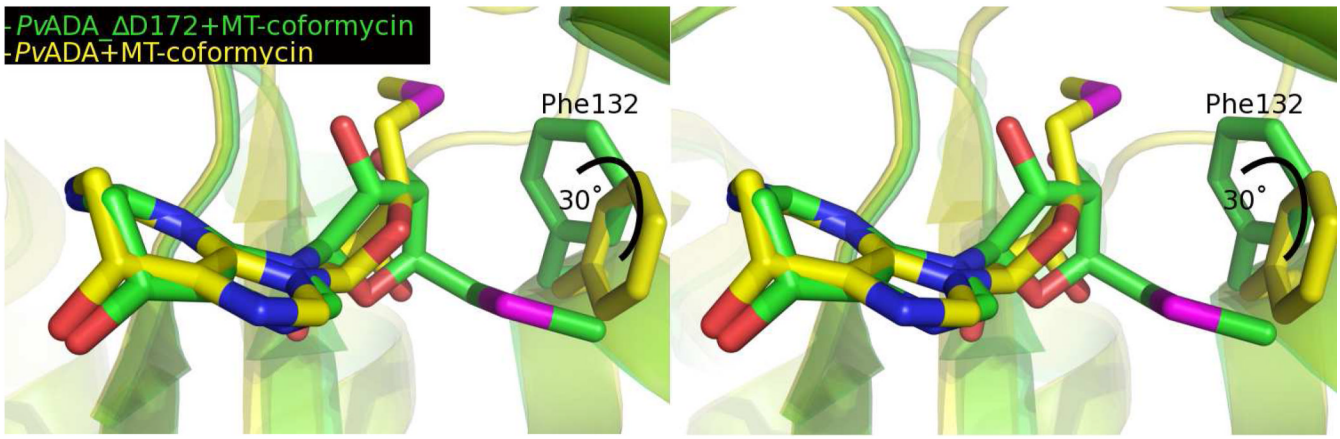

Figure 6.

The stereo view of overlaid structures of MT-coformycin bound to *Pv*ADA or to *Pv*ADA-ΔAsp172. The MT-coformycin and *Pv*ADA are shown in yellow while MT-coformycin in the geometry bound to *Pv*ADA-ΔAsp172 is colored in green. Phe132 rotates approximately 30° to accommodate the methylthio group.

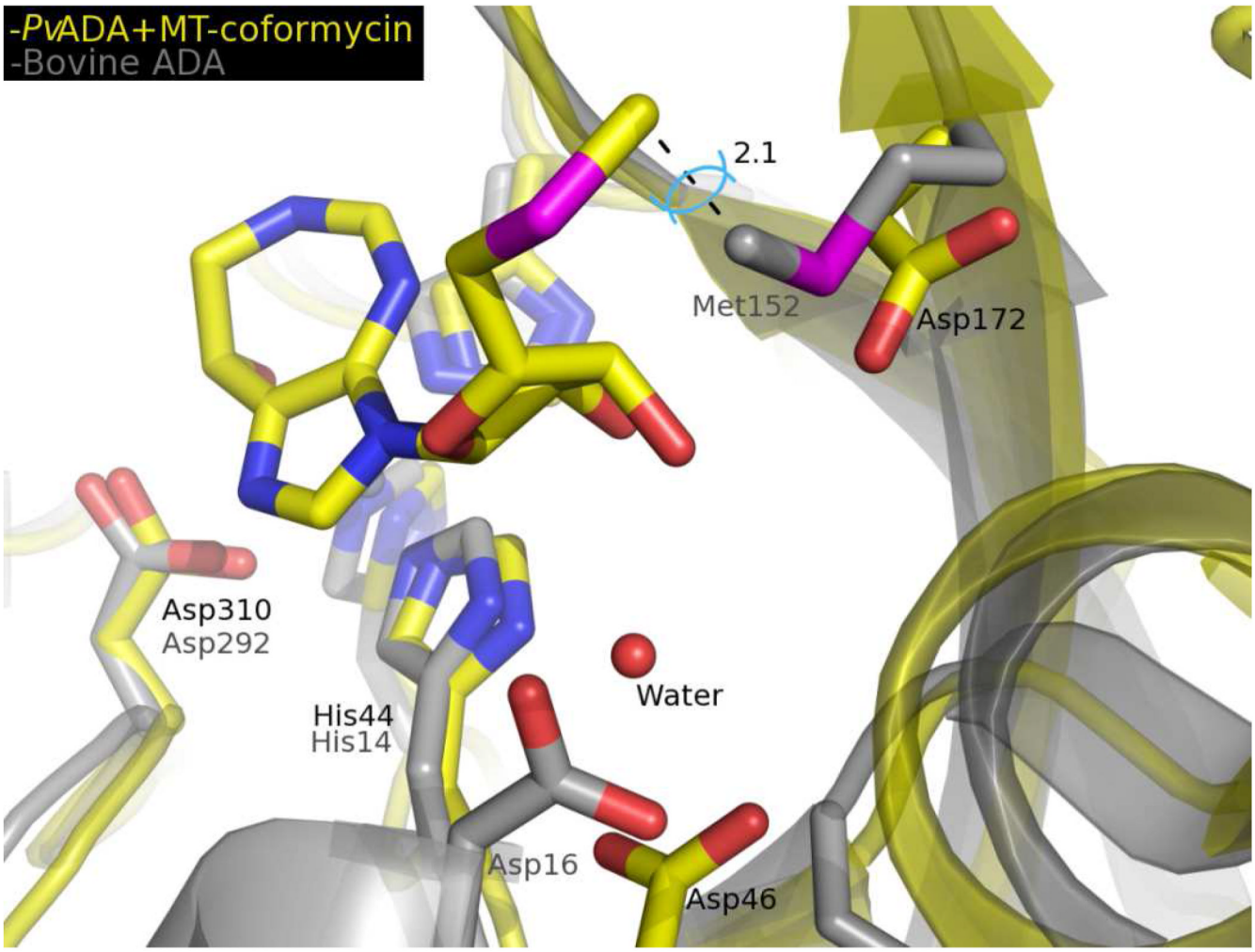

Figure 7.

Overlaid catalytic site residues from *Pv*ADA with bound MT-coformycin are compared to bovine ADA with bound 6-hydroxy-1,6-dihydropurine riboside. Only the MT-coformycin ligand is shown (colored in yellow). Residues from bovine ADA (PDB ID: 1KRM) are shown in gray. The van der Waals overlap between the methylthiol group from MT-coformycin and from the Met at the catalytic site of bovine ADA is shown to be 2.1 in Å. The residues of *Pv*ADA and bovine ADA are labeled in yellow and gray, respectively.

Table 1

X-ray Data Collection and Refinement Statistics.

PDB codes	*Pv*ADA in complex with MT-coformycin 3EWC	*Pv*ADA -ΔAsp172 in complex with MT-coformycin 3EWD
Data collection		
Space group	$P2_12_12$	$P2_12_12_1$
Cell dimension		
a, b, c (Å)	87.0, 100.1, 43.6	41.9, 87.0, 106.1
α, β, γ (°)	90, 90, 90	90, 90, 90
Resolutions (Å)	20-2.0 (2.03-2.00)	20-1.9(1.93-1.90)
Rmerge (%)	15.4 (67.8)	9.7 (67.5)
I / σI	8.8 (1.4)	14.8 (2.4)
Completeness (%)	99.1 (92.0)	99.9 (100)
Redundancy	5.3 (2.7)	2.9 (2.8)
Refinement		
Resolution (Å)	20-2.1	20-1.9
No. reflections (F > 0σF)	21268	29669
Rwork / Rfree (%)	20.4 / 25.4	20.3 / 24.8
B-factors (Å^2)		
Wilson B-factor	24	21
Protein		
(main chain)	25	20
(side chain)	28	23
Water	28	28
Ligand	35	27
R.M.S. deviation from ideality (Å /°)	0.014/1.49	0.018/1.73

[a] Numbers in parentheses show the statistics for the highest resolution shell.

Table 2

Kinetic constants for *Plasmodium* ADAs with adenosine and 5’-methylthioadenosine (MTA) as substrates.

Species	Adenosine			MTA		
	K_m	k_{cat}	k_{cat}/K_m	K_m	k_{cat}	k_{cat}/K_m
	μM	s^{-1}	$M^{-1}\,s^{-1}$	μM	s^{-1}	$M^{-1}\,s^{-1}$
P. vivax	60 ± 6	1.8	3.0×10^4	9.5 ± 0.8	0.13	1.4×10^4
P. falciparum	88 ± 4	5.6	6.4×10^4	115 ± 14	5.8	5.0×10^4
P. cynomolgi	87 ± 9	5.3	6.1×10^4	8.7 ± 0.5	0.31	3.6×10^4
P. knowlesi	120 ± 12	6.8	5.7×10^4	22 ± 3	0.51	2.3×10^4
P. berghei	57 ± 2	4.7	8.2×10^4	4.4 ± 0.6	0.35	7.9×10^4
P. gallinaceum	32 ± 5	1.9	5.9×10^4	ND	ND	ND

ND, Not detected.

Table 3

Inhibition constants of transition state analogue inhibitors for plasmodial ADAs

Species	Coformycin (nM)		MT-Coformycin (nM)	
	K_i	K_i^*	K_i	K_i^*
P. vivax	7.4 ± 0.8	0.71 ± 0.09	20 ± 5	ND
P. falciparum	14 ± 3	0.26 ± 0.03	3.2 ± 0.6	0.25 ± 0.05
P. knowlesi	3.4 ± 0.7	0.64 ± 0.04	48 ± 7	ND
P. cynomolgi	7 ± 2	0.41 ± 0.04	30 ± 3	ND
P. berghei	2.3 ± 0.4	0.15 ± 0.01	14 ± 3	5.0 ± 1.2
P. gallinaceum	4.7 ± 0.7	0.5 ± 0.1	29,000 ± 6000	ND

ND, Not detected. K_i is the dissociation constant for inhibitor during initial rate kinetic measurements. K_i* is the dissociation constant for the inhibitor following a slow-onset tight-binding phase of inhibition.

Table 4

Kinetic and inhibition constants for *Pv*ADA-mutants.

Mutant	Adenosine			Coformycin	
	K_m μM	k_{cat} s^{-1}	k_{cat}/K_m M^{-1} s^{-1}	K_i nM	K_i^* nM
P. vivax (wild type)	60 ± 6	1.8	3.0×10^4	7.4 ± 0.8	0.71 ± 0.09
*Pv*ADA-ΔAsp172	43 ± 5	2.8	6.5×10^4	7.3 ± 0.9	0.60 ± 0.08
*Pv*ADA-Ala172	104 ± 16	14.0	1.3×10^5	1.8 ± 0.5	1.0 ± 0.3
*Pv*ADA-Glu172	83 ± 15	12.9	1.5×10^5	1.5 ± 0.3	0.5 ± 0.1
	MTA			MT-coformycin	
	K_m μM	k_{cat} s^{-1}	k_{cat}/K_m M^{-1} s^{-1}	K_i nM	K_i^* nM
P. vivax (wild type)	9.5 ± 0.8	0.13	1.4×10^4	20 ± 5	ND
*Pv*ADA-ΔAsp172	ND	ND	ND	4,100 ± 1,500	ND
*Pv*ADA-Ala172	ND	ND	ND	ND	ND
*Pv*ADA-Glu172	ND	ND	ND	> 5,000	ND

ND, Not detected.

Table 5

Glycosyl torsion angles

	Dihedral angle (O4'-C1'-N9-C4) or (O4'-C1'-N10-C3)	**PDB ID**
*Pv*ADA in complex with adenosine	−121.2°	2PGF
*Pv*ADA in complex with d-coformycin	−122.4°	2PGR
*Pv*ADA in complex with MT-coformycin	107.3°	3EWC
*Pv*ADA-ΔAsp172 in complex with MT-coformycin	−144.7°	3EWD